1	Key Role of Nitrogen-containing Oxygenated Organic
2	Molecules (OOMs) in SOA Formation Evidenced by OH/NO ₃ -
3	induced Terpinolene Oxidation
4	
5	
6	
7	
8	Hongjin Wu ¹ , Juan Dang ^{1*} , Xiaomeng Zhang ¹ , Weichen Yang ¹ , Shuai Tian ² , Shibo
9	Zhang ^{1*} , Qingzhu Zhang ¹ , Wenxing Wang ¹
10	
11	1. Environment Research Institute, Shandong University, Qingdao 266237, China
12	2. Department of Cardiology, The Eighth Affiliated Hospital, Sun Yat-sen University,
13	Shenzhen, Guangdong 518033, China
14	
15	
16	
17	
18	
10	
19	Keywords: Oxygenated organic molecules; Terpinolene; SOA formation; Atmospheric
20	oxidation; Atmospheric chemical model
21	
2223	
24	
25	
26	
27	*Corresponding author.
28	E-mail address: zhangshibo@sdu.edu.cn (Shibo Zhang); dangj@sdu.edu.cn (Juan
29	Dang)
30	1

Abstract

31

3233

34

35

3637

38

39

40 41

42

43 44

45

46

47 48

Oxygenated organic molecules (OOMs), generated from the oxidation of various biogenic volatile organics with diverse yields, are a great contributor to SOA formation. Terpinolene is an isomeride of limonene, with a high SOA yield. Herein, we investigated the elaborate oxidation mechanism of terpinolene by OH and NO₃, elucidating the new formation mechanism of OOMs and their yield profiles based on the newly-built zero-dimensional chemical model under three typical atmospheric conditions. For terpinolene oxidation by OH, H shift imposes restrictions on continuous autoxidation, instead by the reactions with HO₂/NO/NO₂ resulting in chain termination. For the reaction of terpinolene with NO₃, the transfer of the radical center via bond breaking, triggering a new round of autoxidation, is newly found to be pivotal in the formation of organic nitrate (RONO₂) OOMs with high yields. The effective saturation concentration (C*) of RONO2 OOMs is mostly lower than the OOMs formed by OH oxidation, more easily distributed into the particle phase. The estimated C* of the generated OOMs is distinctly varied among OOM isomers, which emphasizes the necessity of determining their molecular structures, peculiarly the number of rings. The comparative analysis of OH-initiated (daytime) and NO₃-driven (nocturnal) terpinolene oxidation mechanism, highlighted the formation of RONO2 OOMs, would be conducive to molecular structure identification of OOMs in atmospheric monitoring and atmospheric chemical model refinement.

4950

51

52

53

1 Introduction

55

56

57

58

59

60

61

62

63

64

65

66

67

68

69

70

71

72

73

74

75

76

77

78

79

80

81

82

83

In the atmosphere, the multi-generation oxidation reactions of biogenic or anthropogenic volatile organics lead to the formation of oxygenated organic molecules (OOMs) and highly oxygenated organic molecules (HOMs), which are important contributors to secondary organic aerosol (SOA) formation. Given the low volatility, HOMs and OOMs could participate in the nucleation of new particles or condense on the particulate matter to enhance SOA formation. It is well known that SOA has a significant impact on air quality and climate change through scattering and absorbing solar radiation, and serving as cloud condensation nuclei (Shen et al. 2022). Hence, clarifying the formation mechanism of OOMs/HOMs is a vital issue for atmospheric chemistry. Numerous C10OOMs are generated from monoterpenes (C₁₀H₁₆), which are one of the most abundant OOM species in the forests (Bianchi et al. 2017). For instance, the percentage of monoterpene-derived OOMs can be up to 76% in a forested area of southern boreal Finland (Qiao et al. 2023). In urbanized areas of eastern China, the increase in vegetational cover generates a mix of anthropogenic and biological emissions, which contribute to SOA formation (Wang et al. 2020), suggesting that monoterpene OOMs are of concern in urban areas, not only in forested areas (Huang et al. 2016). Concretely, monoterpene OOMs have been detected in recent urban atmospheric observations, approximately 30% of the particulate generation below 10 nm is attributed to monoterpene OOMs in Nanjing (Huang et al. 2016). Measurements in forested areas revealed that monoterpene oxidation products played a dominant role in driving new particle growth (Huang et al. 2016, Mohr et al. 2019), while the atmospheric oxidation mechanisms of monoterpenes, especially the formation of OOMs, have not been fully elucidated.

Previous research mainly focused on the molecular composition (Guo et al. 2022, Liu et al. 2021, Nie et al. 2022), the information on the molecular structure is limited, which hindered a well-grounded understanding of the atmospheric fate of OOMs (Bianchi et al. 2019, Garmash et al. 2020, Kurtén et al. 2017). For instance, when trying to identify the OOMs detected from the field observation, 151 chemical formulas could be categorized as monoterpenes or aromatic hydrocarbons, which would lead to the deviations in OOMs detection and SOA formation

estimation (Qiao et al. 2023). In addition to forming new particles, the relative contribution of OOMs to SOA formation is governed by their net condensation potential, primarily determined by vapor concentrations and volatility (Wang et al. 2022). Generally, the higher the oxygen content of OOMs, the lower their volatility. Given the lack of pure standards, especially for complex multifunctional oxidation products such as OOMs, the measured saturated vapor pressure data are extremely limited. Therefore, the field observations and laboratory studies have employed a two-dimensional volatility basis set (2D-VBS) classification framework to identify the key SOA-contributing components by combining the effective saturation concentration (C*) and the oxidation state of the oxidation products. In addition, the volatility of the organics with the same molecular formula could vary dramatically due to the structural difference in the functional groups and hydrogen bond (Bianchi et al. 2019, Vasudevan-Geetha et al. 2024). For the estimation of the vapor pressure, Isaacman-VanWertz and Aumont (2021) assumed that the impact of a nitrate group on the vapor pressure is equivalent to a hydroxyl group, which was considered reasonable for the reaction system dominated by R-ONO2 and peroxynitrates in organic nitrogen gas-phase oxidation products. Besides, according to the chamber experiments and structure-activity relationships, adding -ONO2 functional groups to C10 and larger molecules could reduce the vapor pressure (Rollins et al. 2013). Currently, the molecular structures of OOMs have not been adequately determined in the field measurements and laboratory investigations, the assessment of their volatility deserves further research.

84

85

86

87

88

89

90

91

92

93

94

95

96

97

98

99

100

101

102

103

104

105

106

107

108

109

110

111

112

113

The atmospheric models typically only consider the representative monoterpene (such as α-pinene), but the SOA yields of different monoterpenes vary widely even with analogous structure (Draper et al. 2015, Friedman and Farmer 2018, Fry et al. 2014, Kurtén et al. 2017, Vasudevan-Geetha et al. 2024). In this work, terpinolene is selected as a model compound due to its high SOA yield. As a kind of cyclic diolefins with an endocyclic and an exocyclic double bond(Griffin et al. 1999), terpinolene has an atmospheric lifetime of 2 hours or less (Corchnoy and Atkinson 1990). The estimated annual emission of terpinolene is roughly 1.3 Tg yr⁻¹ (Guenther et al. 2012, Reissell et al. 1999), which is emitted by deciduous tree species such as Sophora japonica and Ginkgo biloba, as well as medicinal plants like Amomum tsaoko seeds (Lindwall et al. 2015). The previous studies have investigated the reaction of terpinolene with O₃ by experimental or theoretical methods (Aschmann et al. 2002, Atkinson et al. 1992,

Atkinson et al. 1990, Herrmann et al. 2010, Kim 2016, Lee et al. 2006, Luo et al. 1996, Orzechowska 2003, Shu and Atkinson 1994, Witter et al. 2002). For the reaction of OH with terpinolene, the rate constant is 2.25×10⁻¹⁰ cm³molecule⁻¹s⁻¹ (Corchnoy and Atkinson 1990, Griffin et al. 1999), and the yields of two main products, acetone (32~39%) and 4-methyl-3cyclohexen-l-one (~26%), have been determined (Hakola et al. 1994, Orlando et al. 2000, Reissell et al. 1999). Notably, the OH-initiated oxidation of terpinolene demonstrates a distinctly higher SOA yield (33% at 5.7 days aging time) compared to α-pinene and limonene (Friedman and Farmer 2018, Surratt et al. 2008). Except for the daytime atmospheric oxidation induced by OH and O₃, NO₃-initiated reactions have been identified as a pivotal nocturnal pathway for terpinolene, with a rate constant of $(6.0\pm3.8)\times10^{-11}$ cm³molecule⁻¹s⁻¹ (Fouqueau et al. 2022). Experimental studies have identified first- and second-generation oxidation products (such as $C_{10}H_{16}O_3$ and $C_8H_{17}N_2O_4$) and proposed that the oxidation mechanism of terpinolene initiated by NO₃ is dominated by NO₃ addition (Fouqueau et al. 2022), with the SOA yield of up to 60% (Corchnoy and Atkinson 1990, Fouqueau et al. 2022, Griffin et al. 1999, Martínez et al. 1999, Stewart et al. 2013). As an important precursor for SOA formation, the OOMs formation mechanisms derived from terpinolene remain unclear, which is critical for deepening the understanding of SOA formation and refining the atmospheric models.

In this study, we combined oxidation mechanism investigation and newly-built kinetic modeling to systematically elaborate OOMs formation from terpinolene oxidation initiated by OH and NO₃ radical, illustrating the yield profiles of OOMs and other products. Additionally, we utilized the functional group contribution method and the molecular formula parameterization method to estimate the saturated vapor pressures of the OOMs to evaluate their contribution to NPF and SOA formation. The comparative investigation of OH-initiated and NO₃-driven oxidation mechanisms of terpinolene, especially for the formation of OOMs, is expected to fill the gap between ambient monitoring of SOA and atmospheric model forecasts.

2 Methods

114

115

116

117

118

119

120

121

122

123

124

125

126

127

128

129

130

131

132

133

134

135

136

137

138

139

140

141

142

2.1 Electronic structure and energy calculations

All the quantum chemical calculations were performed utilizing Gaussian 16 software. Conformational optimizations for the reactants, intermediates, transition states, and products were all carried out at the M06-2X/6-31+G(d, p) computational level. Intrinsic reaction coordinate (IRC) was conducted to ensure that the transition states were related to the matching reactants and products at the same computational level. The single point energies were calculated at M06-2X/6-311++G(3df,3pd) level enhanced the accuracy of energies. The distribution of average local ionization energies (ALIE) was plotted using Multiwfn (Lu and Chen 2012) combined with VMD (Humphrey et al. 1996) for terpinolene to specify its electronrich sites.

2.2 Kinetics calculations

The rate constants of the reactions are calculated by transition state theory, with the tunneling effect corrected by the Wigner method. The pseudo-first-order rate constants for the bimolecular reactions were derived from the rate constants of RO₂ radicals with HO₂/NO/NO₂ and the concentrations of the reactants under the atmospheric conditions of the urban, suburban, and forested areas. The reaction rate constants were all calculated at 298 K, 1 atm. Using MATLAB, the zero-dimensional chemical models are established based on the oxidation mechanism and kinetics of the alkyl radicals (Ter-R•) produced by the reactions of terpinolene with OH and NO₃ radical.

2.3 Vapor prediction

The functional group contribution method (SIMPOL.1) was used to predict the saturation vapor pressures based on the molecular structure and functional groups of the OOMs (Pankow and Asher 2008). In addition, the molecular formula parameterization method is also employed to calculate the effective saturation concentration(C*) of the OOMs, which was optimized by Mohr et al. (Mohr et al. 2019) based on the HOMs dataset (Tröstl et al. 2016). The details of these methods are provided in the Supporting Information S1.

3 Results and discussion

For the clarity of the molecular structure and reaction pathways, the carbon atoms of terpinolene were labeled as shown in Fig. S1. Analysis of the ALIE distribution revealed that the two double bonds exhibit the lowest ALIE values, indicating their highest reactivity as the primary reactive sites.

3.1 Initial reactions of Terpinolene with OH/NO₃ radical

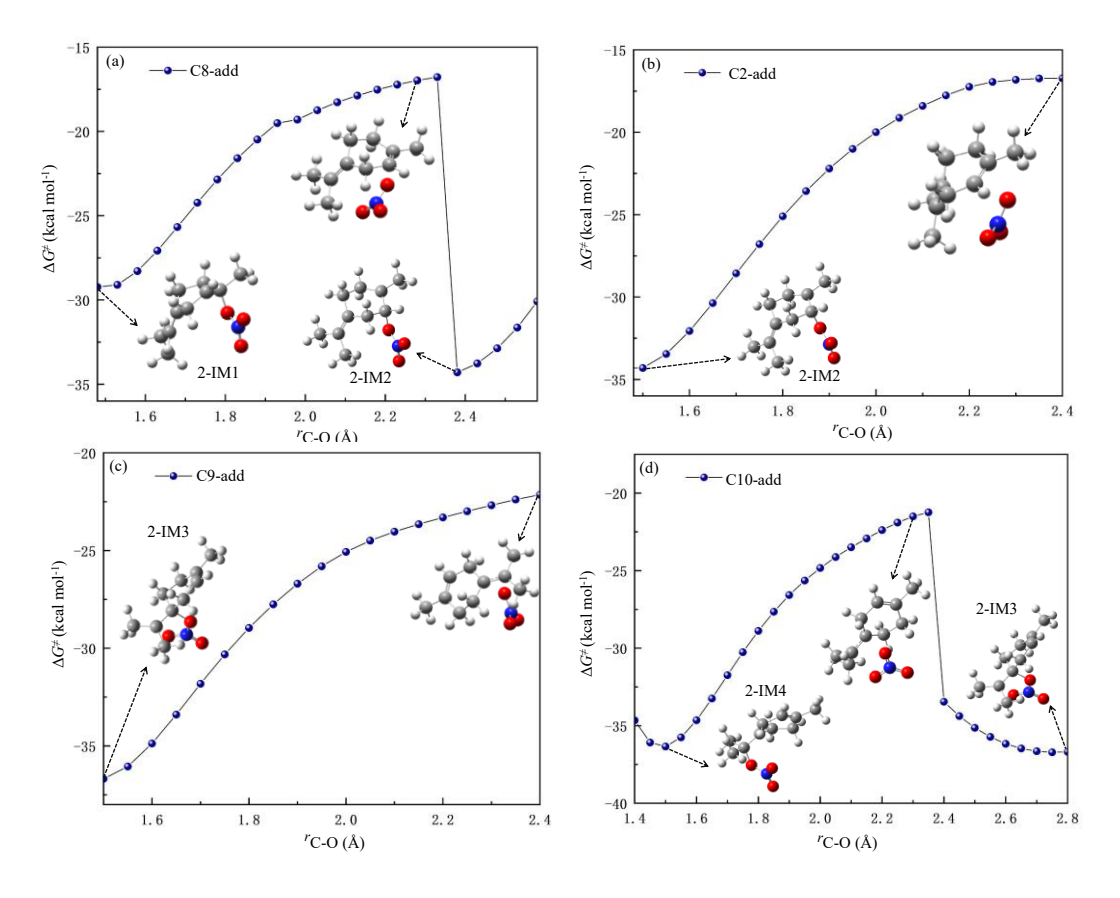


Figure 1. Scanned potential energy surfaces for NO₃ radical addition reactions (unit in kcal mol⁻¹)

The initial reactions of terpinolene with OH radical primarily proceed via two mechanisms (Fig. S2), i.e., OH radical addition to two nonconjugated double bonds and H-abstraction by OH radical. All the addition reactions are exergonic and thermodynamically feasible in the atmosphere with the energy barriers of $1.9 \sim 4.7$ kcal mol⁻¹, leading to the formation of OH-terpinolene adducts. Analogous to addition reactions, the H-abstraction processes are all exergonic with small free energy barriers ($4.9 \sim 9.0$ kcal/mol), yielding seven alkyl radicals. The OH addition is dominant over the H-abstraction reaction pathway, which is consistent with the previous laboratory studies (Arey et al. 1990, Orlando et al. 2000, Reissell et al. 1999).

Similar to OH radical, NO₃ radical addition and H-atom abstraction from the carbon chain by NO₃ radical are the initial reaction pathways of terpinolene with NO₃. Notably, NO₃ radical migration is observed in NO₃ addition processes, as shown in the potential energy surface scans at the M06-2X/6-311++G(3df, 3pd) computational level in Fig. 1 (a) and (d), the addition of NO₃ radical to C8 and C10 site produce 2-IM1 and 2-IM4, respectively, which then undergo NO₃ migration to generate 2-IM2 and 2-IM3, overcoming low energy barriers. According to

Fig. 3 (b) and (c), the energy increases with the gradual rising distance of the C-O bond without a saddle point. Therefore, these two addition reactions are considered as barrierless processes. Regarding the H abstraction by NO_3 radical, it can be seen from Fig. S3 that the abstraction reactions are all exothermic (-0.7 \sim -27.8 kcal mol⁻¹), crossing the energy barriers of $1.2 \sim 16.4$ kcal mol⁻¹ to produce seven different radical intermediates.

3.2 The oxidation of alkyl radicals (Ter-R•) initiated by OH/NO3 radical

3.2.1 The oxidation of OH-Terpinolene-R• (1-IM4 and 1-IM7)

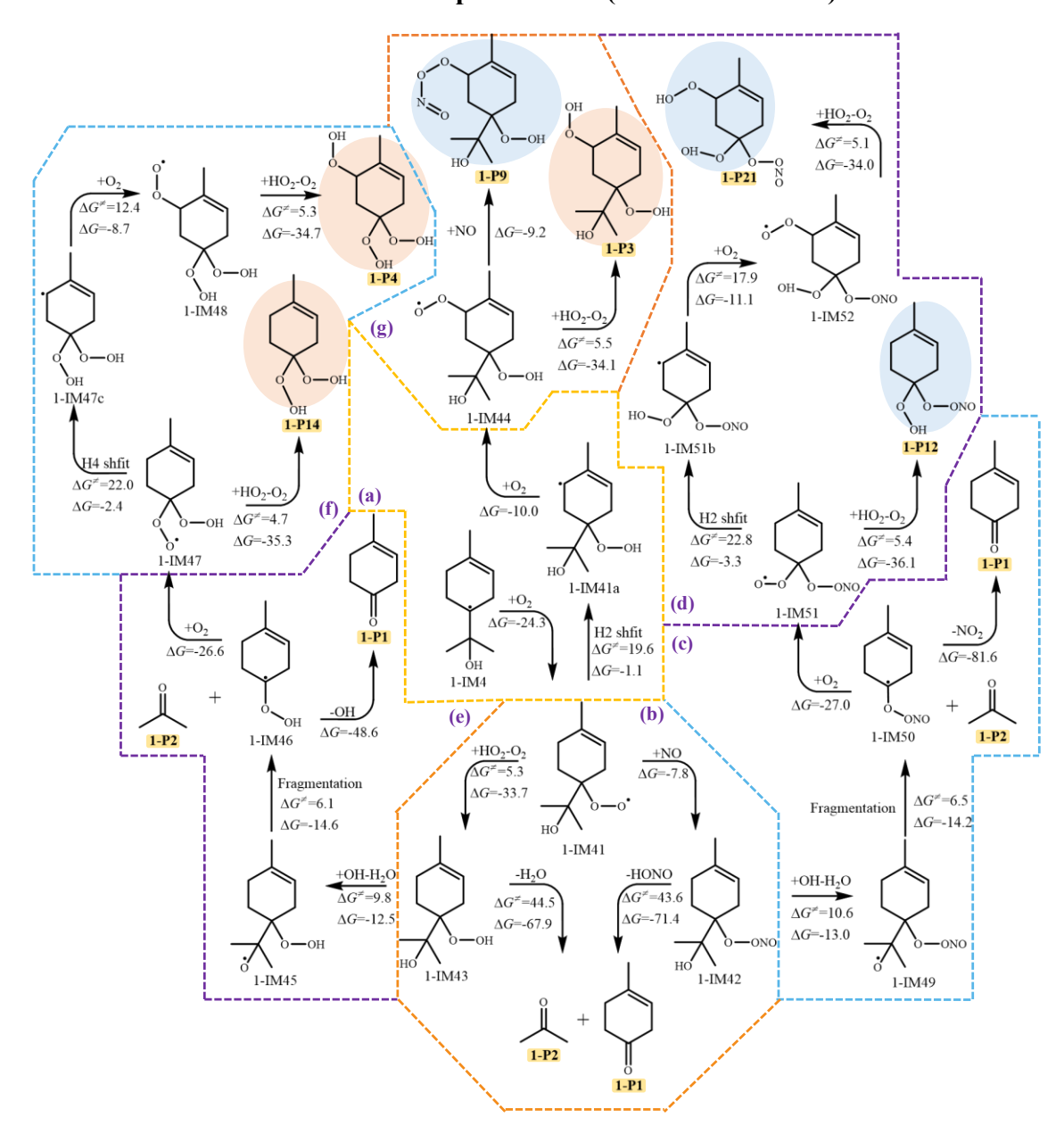


Figure 2. The subsequent reactions of OH-Ter-R• (1-IM4) (unit in kcal mol⁻¹, RONO₂ OOMs marked in light blue, nonnitrogenous OOMs marked in lightsalmon)

The alkyl radicals (1-IM4 and 1-IM7) were selected for in-depth study of the atmospheric oxidation mechanism, which are the dominant intermediates formed from OH addition and Habstraction reactions, respectively. Similar to other C-centered radicals, the reaction with O₂ is the main pathway of 1-IM4 (Peeters et al. 2014). As shown in Fig. 2, 1-IM4 undergoes a rapid barrierless association reaction with O₂, which is exoergic by 24.3 kcal mol⁻¹, leading to the generation of 1-IM41. Three competitive reaction pathways of 1-IM41 are considered: conjugation reaction with NO to generate 1-IM42 under high NO_x conditions, reaction with HO₂ to form the intermediate 1-IM43 under the atmospheric condition of low NOx, and the isomerization reactions, including the cyclization and hydrogen shift. The aforementioned reactions of 1-IM42 and 1-IM43 can both generate 1-P1 and 1-P2, which have been detected in laboratory studies of the reaction of terpinolene with OH radical (Hakola et al. 1994). Unlike the formation mechanism of 1-P2 in the previous experimental research, which proposed that the intermediate generated by the association with NO could directly lead to the formation of 1-P2 and 1-P1 through the removal of NO₂ (Fig. S4) (Orlando et al. 2000, Reissell et al. 1999), we found that HONO is eliminated from 1-IM42 other than NO₂, with a relatively high energy barrier. In addition, 1-IM42 can also undergo H-atom abstraction by OH and the C-C bond cleavage to generate 1-IM50, followed by the elimination of NO₂, yielding 1-P1 and 1-P2. Similarly,1-IM43 can either undergo the removal of H₂O or H-atom abstraction, followed by the fragmentation of the C-C and O-O bond, leading to the formation of the new C7 alkyl radicals (1-IM46), 1-P1 and 1-P2, of which, by comparing the energy barriers, the latter pathway is easier to occur under atmospheric conditions. As depicted in Fig. 2(d),1-IM50 can further react with O₂ to generate the peroxyl radical 1-IM51, which then reacts with HO₂ to generate 1-P12 or triggers a new round of autoxidation, with H2 shift (1,5 H shift) as the ratedetermining step, leading to the formation of 1-P21. Analogously, 1-IM46 can undergo O₂ addition to generate a peroxyl radical 1-IM47, ultimately resulting in the generation of 1-P4 and 1-P14. According to the traditional autoxidation mechanism (Fig. 2(a)), 1-IM41 undergoes H2 shift (1,5 H shift) to form 1-IM41a with an energy barrier of 19.6 kcal mol⁻¹, which further reacts with O₂ to produce a new peroxyl radical 1-IM44. Whereas, the subsequent oxidation of 1-IM44 is restricted due to the high energy barriers of the H shift and cyclization reactions (Fig. S6), which cannot occur spontaneously under atmospheric conditions. Therefore, 1-IM44 can

199

200

201

202

203

204

205

206

207

208

209

210

211

212

213

214

215

216

217

218

219

220

221

222

223

224

225

226

227

only react with HO₂ to form 1-P3 or react with NO to produce a nitrogenous OOM 1-P9, which have been identified as the major monoterpene-derived C10OOMs in the field observations (Guo et al. 2022, Luo et al. 2023, Zheng et al. 2023). The presence of the endocyclic double bond enables 1-IM41 to undergo cyclization to generate 1-IM41f and 1-IM41g, which are thermodynamically unfavorable under atmospheric conditions (Fig. S5).

229

230

231

232

233

234

235

236

237

238

239

240

241

242

243

244

245

246

247

248

249

250

251

The subsequent reaction pathway of 1-IM7 is initiated with O₂ addition to form the peroxyl radical 1-IM71, which further reacts with HO₂ to generate 1-IM74, followed by the hydrogen abstraction by OH radical and OH elimination to yield 1-P7 (Fig. 3(b)). 1-IM71 can also react with NO, consecutively proceeding with NO₂ elimination and the binding with O₂ to produce the peroxyl radical 1-IM78. As shown in Fig. 3(c), 1-IM78 can sequentially react with HO₂/NO to generate 1-P8 and 1-P11, respectively. In addition, 1-IM78 can also undergo H4 shift (1,6 H shift) to form 1-IM78d, which subsequently reacts with O₂ to generate a new peroxyl radical 1-IM79, eventually leading to the production of 1-P13, which has been detected in the field observation and the laboratory studies of limonene oxidation by OH (Luo et al. 2023, Zheng et al. 2023). Furthermore, the peroxyl radical 1-IM79 can react with NO/NO₂ to produce organic nitrate (RONO₂) OOMs 1-P15 and 1-P16. Additionally, the peroxyl radical 1-IM71 undergoes the H4 shift (1,5 H shift) and the association with O₂ to produce a new peroxyl radical 1-IM72, which can further react with HO₂ to generate the OOM 1-P5, or react with NO/NO₂ to form 1-P17 and 1-P18, respectively (Fig. 3(e)). Analogously, Fig. 3(f) indicates that the peroxyl radical 1-IM72 can undergo a subsequent H4 shift (1,5 H shift) reaction, initiating an additional autoxidation cycle to generate more OOMs. The isomerization reactions involved in the reaction pathways are displayed in Section. S3 of Supporting Information, and the major products from the reactions of terpinolene with OH/NO₃ are summarized in Sect. S6.

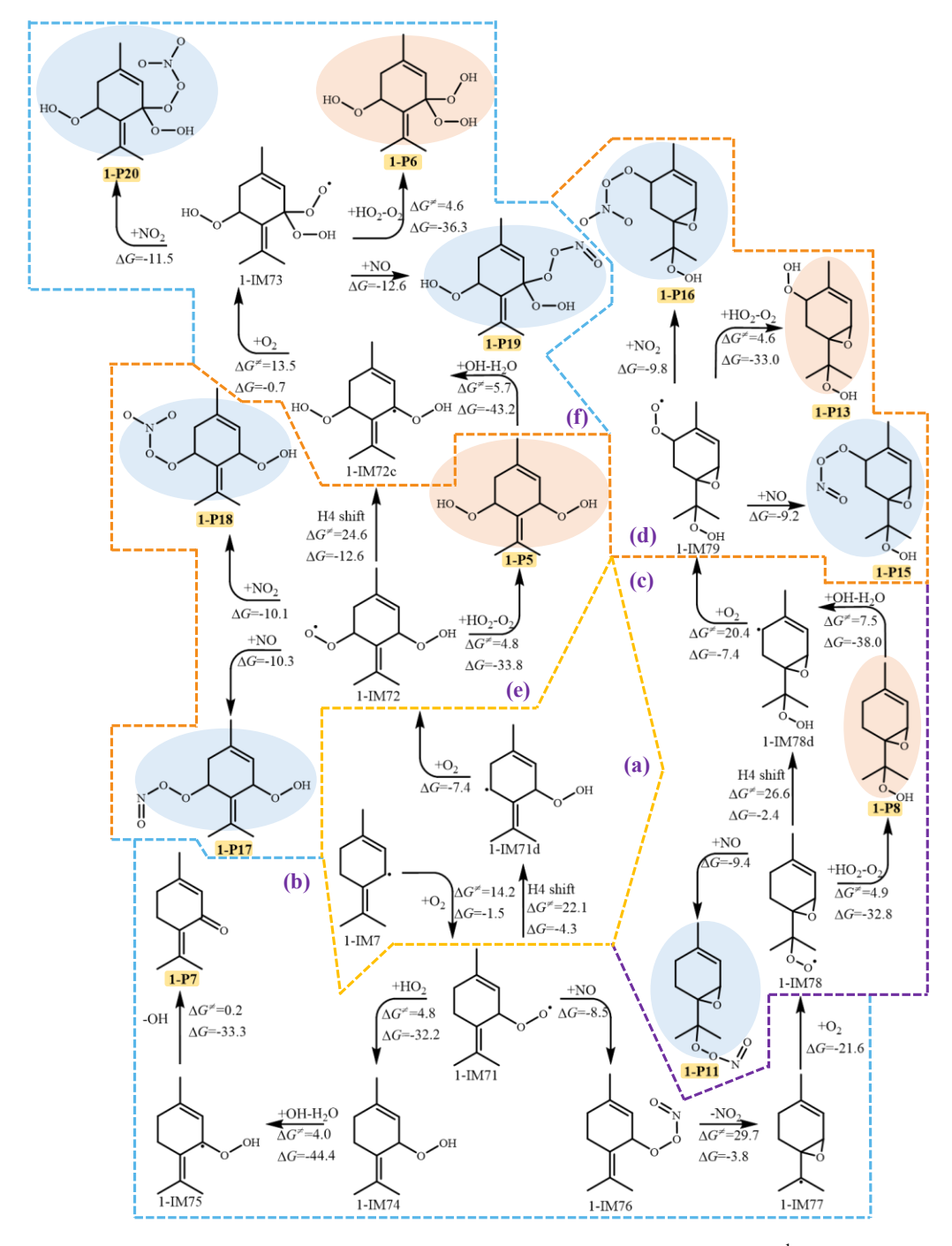


Figure 3. The subsequent reactions of OH-Ter-R• (1-IM7) (unit in kcal mol⁻¹, RONO₂ OOMs marked in light blue, nonnitrogenous OOMs marked in lightsalmon)

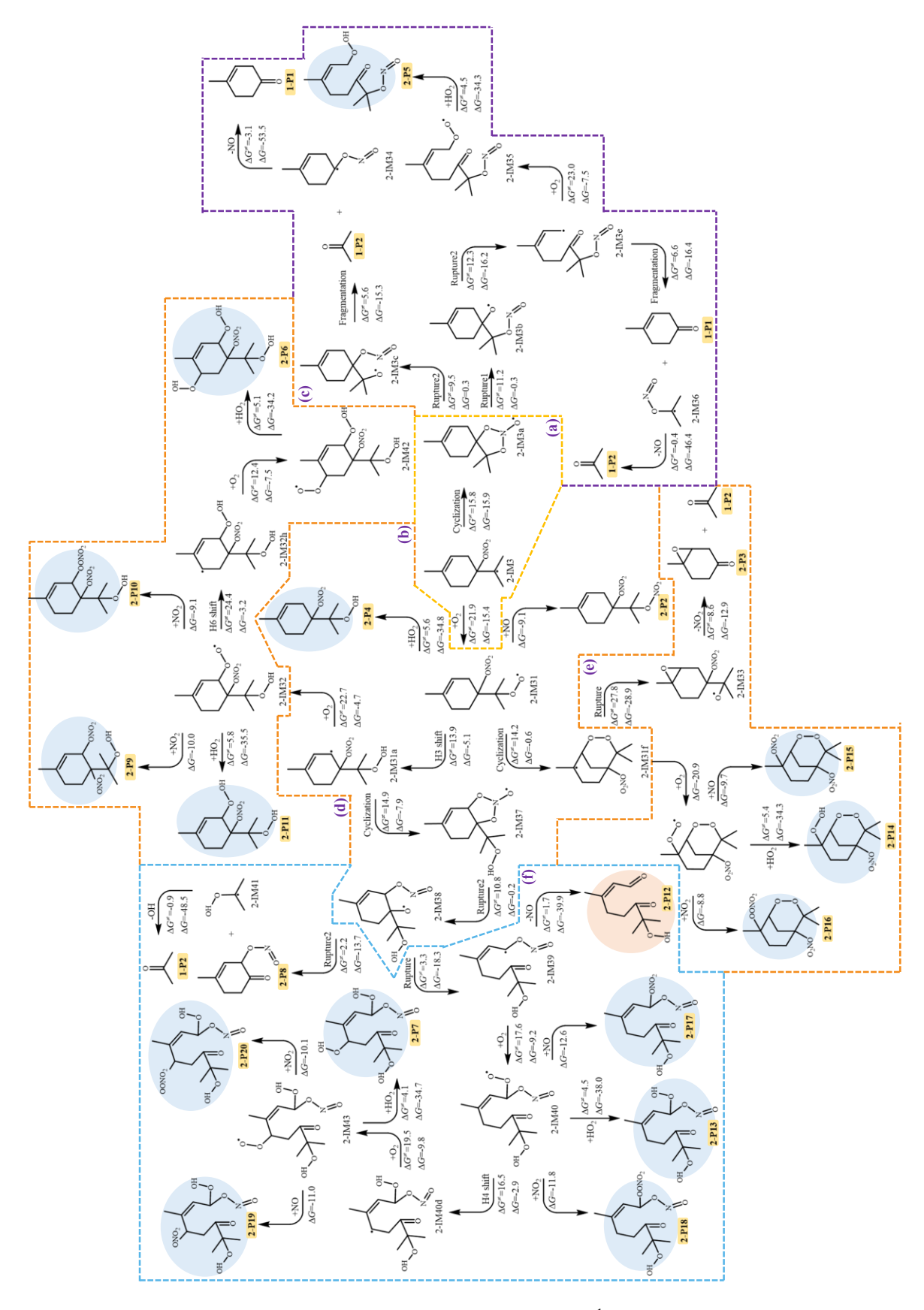


Figure 4. The subsequent reactions of NO₃-Ter-R• (2-IM3) (unit in kcal mol⁻¹, RONO₂ OOMs marked in light blue, nonnitrogenous OOMs marked in light salmon)

3.2.2 The atmospheric oxidation of the NO₃-Terpinolene-R• (2-IM3)

258

259

260

261

262

263

264

265

266

267

268

269

270

271

272

273

274

275

276

277

278

279

280

281

282

283

284

285

286

The dominant intermediate NO₃-Ter-R• (2-IM3) is prone to cyclization to form a bicyclic alkoxyl radical (2-IM3a), as shown in Fig. 4. Due to the instability of the N-O bond, 2-IM3a undergoes the rupture of the O-N bond to produce 2-IM3b or 2-IM3c, which both subsequently proceed with the fragmentation and NO elimination to generate 1-P1 and 1-P2. Besides, Fig. 4(c) indicates that the radical center of 2-IM3b migrates from the oxygen atom to the carbon atom via C-C bond breaking, and consecutively reacts with O2 and HO2 to generate 2-P5. Similar to the intermediate OH-Ter-R• (1-IM4), 2-IM3 also reacts with O₂ to generate the firstgeneration peroxyl radical (2-IM31), which further reacts with HO₂ to generate 2-P4 (Fig. 4(b)). As the presence of an endocyclic double bond, 2-IM31 proceeds with the cyclization to produce 2-IM31f with a barrier of 14.2 kcal mol⁻¹, followed by O-O bond rupture and NO₂ removal to form 2-P3 and 1-P2, which have been detected in the laboratory studies for the oxidation of terpinolene by NO₃ radical (Fouqueau et al. 2022). Moreover, as shown in Fig. 4(e), the bicyclic alkyl radical 2-IM31f ulteriorly reacts with O₂ to form a new peroxyl radical, resulting in the formation of multiple OOMs. Among all the H shift reaction pathways (Fig. S11), H3 shift (1,5 H shift) is the dominant reaction pathway to form 2-IM31a, which continues to react with O₂ to produce 2-IM32 or proceeds with a cyclization reaction to generate an alkoxy radical 2-IM37. The peroxyl radical 2-IM32 can further undergo the bimolecular reactions with HO₂/NO/NO₂, or continue the autoxidation to produce 2-P6, as shown in Fig. 4(d). For the subsequent reactions of the alkoxy radical 2-IM37, the cleavage of the O-N and C-C bond occurs, followed by OH removal, leading to the formation of 2-P8 and 1-P2. In addition, 2-IM37 can also undergo the rupture of the O-N and C-C bonds to produce the intermediate 2-IM39, which can react with O2 or eliminate NO to generate a new peroxyl radical 2-IM40 or 2-P12. Subsequently, 2-IM40 proceeds with the autoxidation mechanism driven by H4 shift (1,6-H shift) and then the reaction with HO₂ to generate 2-P7 and 2-P13. The peroxyl radicals (2-IM40 and 2-IM43) can also react with NO/NO₂ to produce RONO₂ OOMs, including 2-P17, 2-P18, 2-P19, and 2-P20. According to the field observation of OOMs at a coastal background site in Hong Kong, 2-P6 and 2-P9~2-P20 have been detected (Zheng et al. 2023). Moreover, the MT-mixed-OOMs identified in the

atmospheric monitoring over eastern China's megacities, such as 2-P9, 2-P10, 2-P15 \sim 2-P18, are considered to be generated by the reactions of the peroxyl radicals with NO/NO₂, which is in accordance with the reaction pathways we discussed above (Liu et al. 2023). For clarity, the above-mentioned products that could have been detected in field observations are all summarized in the Supplementary Section. S6.

287

288

289

290

291

292

293

294

295

296

297

298

299

300

301

302

303

304

305

306

307

308

309

3.3 Modeling of the yield profiles of OOMs and other main products

Based on the aforementioned oxidation mechanism of terpinolene by OH and NO₃ radical, the thermodynamically feasible reaction pathways were determined, and a zero-dimensional chemical model was further established to calculate the time-dependent fractional yields of the intermediates and major products including OOMs under three atmospheric conditions: (a) in a urban area (50 ppb NO, 39 ppb NO₂, 1 ppt HO₂), (b) in a suburban area (3 ppb NO, 9 ppb NO₂, 3 ppt HO₂), and (c) in a forested area (0.5 ppb NO, 4 ppb NO₂, 40 ppt HO₂) (Guo et al. 2024, Kieloaho et al. 2013, Klemm et al. 2006, Lew et al. 2020, Ma et al. 2019, Mao et al. 2010, Mavroidis and Ilia 2012, Mazzeo et al. 2005, Zhang et al. 2022). Based on the bimolecular reaction rate constants of the RO₂ with NO $(9.0 \times 10^{-12} \text{ cm}^3 \text{ molecule}^{-1} \text{ s}^{-1})$, NO₂ $(1.10 \times 10^{-11} \text{ s}^{-1})$ cm³ molecule⁻¹s⁻¹) and HO₂ (1.7 × 10⁻¹¹ cm³ molecule⁻¹ s⁻¹) and the C-centered radicals with O₂ $(6.0 \times 10^{-12} \text{ cm}^3 \text{ molecule}^{-1} \text{s}^{-1})$ (Atkinson and Arev 2003, Boyd et al. 2003, Saunders et al. 2003. Wang and Wang 2016, Wu et al. 2015), the pseudo-first-order rate constants were determined and inputted into the model, as summarized in Supplementary Sect. S4. In the urban area, the calculated pseudo-first-order rate constant $k'_{\text{RO2+NO}}$ (1.11× 10¹ s⁻¹) is significantly larger than $k'_{\text{RO2+HO2}}$ (4.18 × 10 ⁴ s⁻¹). Whereas, under the atmospheric condition of the forested area, where NO concentration is 0.5ppb, $k'_{\text{RO2+HO2}}$ (1.67 × 10⁻² s⁻¹) becomes comparable with $k'_{\text{RO2+NO}}$ (1.11 $\times 10^{-1} \, \mathrm{s}^{-1}$).

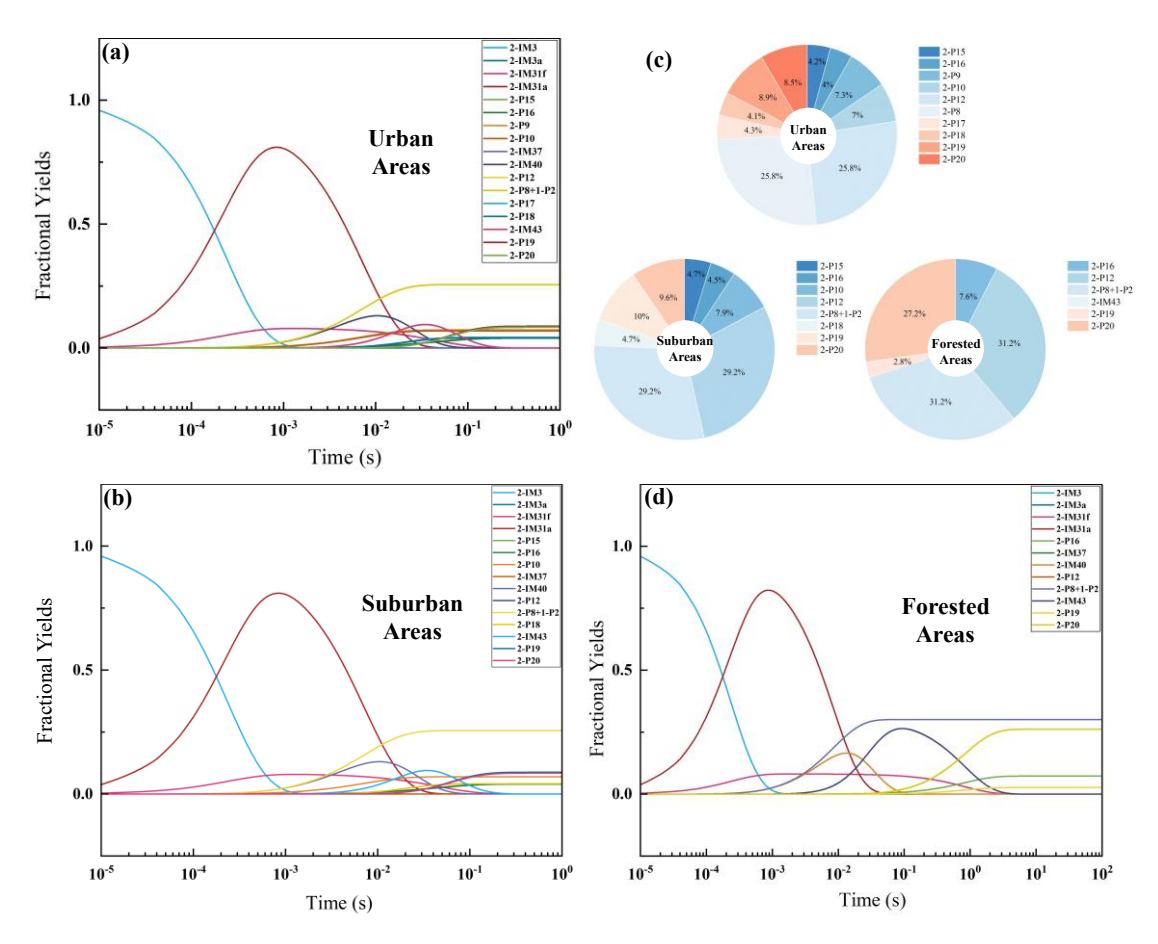


Figure 5. The modeled time-dependent fractional yields of important species generated from the subsequent reactions of NO₃-Ter-R•(2-IM3) under the atmospheric conditions of urban areas (a), suburban areas (b), forested areas (d) (Species with yields 1% excluded).

The time-dependent fractional yield of the major products from the oxidation of NO₃-Ter-R• (2-IM3) is shown in Fig. 5. The rate constants of the rate-determining steps for the generation of 2-IM3a, 2-IM31a, and 2-IM31f from 2-IM3 were calculated to be 27.1 s⁻¹, 3.83 × 10³ s⁻¹, and 3.42×10^2 s⁻¹, respectively. Compared to the bimolecular reaction pathways for the production of 2-P4 and 2-P2, unimolecular reactions are more dominant, among which, 2-IM31a generated by the hydrogen shift reaction is the predominant intermediate. As shown in Fig. 5(a), the fractional yield of 2-IM31a is sharply increased to 80% at $\sim 10^{-3}$ s in the urban area, accompanied by a rise in the yield of 2-IM31f to $\sim 8.0\%$. Subsequently, the yield of 2-IM31a declines rapidly to $\sim 0\%$, along with the rising yield of 2-P8, 2-P12, and 1-P2 to level off at $\sim 26\%$ at 10^{-1} s. Sequentially, 2-IM31a undergoes the cyclization and O₂ addition to produce 2-IM40, which is stabilized at $\sim 13\%$ at around 10^{-2} s. The continuous oxidation of 2-IM40 leads to the increasing yield of 2-IM43 via the autoxidation driven by the H4 shift reaction (4.43 ×

10 s⁻¹). Ultimately, the OOMs 2-P19 and 2-P20 are formed from the reactions of 2-IM43 with NO and NO₂, with their yields leveling off at 1 s. As indicated in Fig. 5 (b) and (d), the intermediates generated by the unimolecular reactions (such as 2-IM31a, 2-IM43, etc.) are also dominant. In urban and suburban areas, the yields of 2-P19 and 2-P20 are comparable; however, in the forest area, 2-P20 generated by the peroxyl radical and NO₂ are the main RONO₂ OOMs, with the yield of 27.2%. Additionally, in the urban area, the yields of 2-P9 and 2-P17 produced by the peroxyl radicals and NO are 7.3% and 4.3%, respectively, while those are all below 1% in suburban and forest areas. The reactions of peroxyl radicals with HO₂ increase the yield of 2-P7(< 1%) in the forest and suburban area, but can't compete with those of peroxyl radicals with NO/NO₂ which leads to the production of 2-P19 and 2-P20. As summarized in Fig. 5 (c), under these three atmospheric conditions, 2-P8, 2-P12, 2-P19, and 2-P20 are the main OOMs with relatively high yields, while 2-P10 is the major OOM in the urban and suburban areas (7% and 7.9%, respectively). The total yield of the OOMs (2-P15 and 2-P16) generated by the subsequent oxidation of 2-IM31f produced by the cyclization reaction is approximately 8~10% in the urban and suburban area, while the OOM in the forested area (2-P16) has a yield of 7.6%. As shown in Fig. S16, as the main oxidation product, the yields of 1-IM42 are 96.8% and 64.1% in the urban and suburban areas, respectively, followed by 1-P9. In the forested area, the main oxidation intermediate of 1-IM4 is 1-IM41a, generated by the first hydrogen shift reaction, which undergoes bimolecular reactions with HO₂/NO to produce 1-P3 (9.7%), 1-P9 (64.7%), 1-IM42 (22.2%), and 1-IM43 (3.3%). In Fig. S17, under three atmospheric conditions, the yield of 1-IM76 is over 80%, synchronously, being one of the main oxidation products. The fractional yield of 1-P7 and 1-P18 is enhanced to 12% and 2%, respectively, in forested areas, By contrast, there is a significant difference in the yields of OOMs produced from the oxidation of terpinolene by OH and NO₃ radical, mainly due to the different oxidation pathways.

3.4 Volatility distribution of OOMs

325

326

327

328

329

330

331

332

333

334

335

336

337

338

339

340

341

342

343

344

345

346

347

348

349

350

351

352

353

The saturation vapor pressures of OOMs can affect their condensation process, which is closely related to SOA formation. Low volatility organic compounds (LVOC) and extremely low volatility organic compounds (ELVOC) have been demonstrated to be a significant contributor to the growth of a large proportion of the new particles, with a minor contribution

from semi-volatile organic compounds (SVOC) (Mohr et al. 2017). Herein, based on the chemical formula and functional groups of the OOMs generated from the oxidation of terpinolene by OH and NO₃, the saturation vapor pressures of the OOMs were firstly predicted using SIMPOL.1 functional group contribution method (Pankow and Asher 2008, Valorso et al. 2011). It was then converted to the effective saturation concentration (C*) for further comparison with the estimation by the optimized molecular formula parameterization method (Mohr et al. 2019).

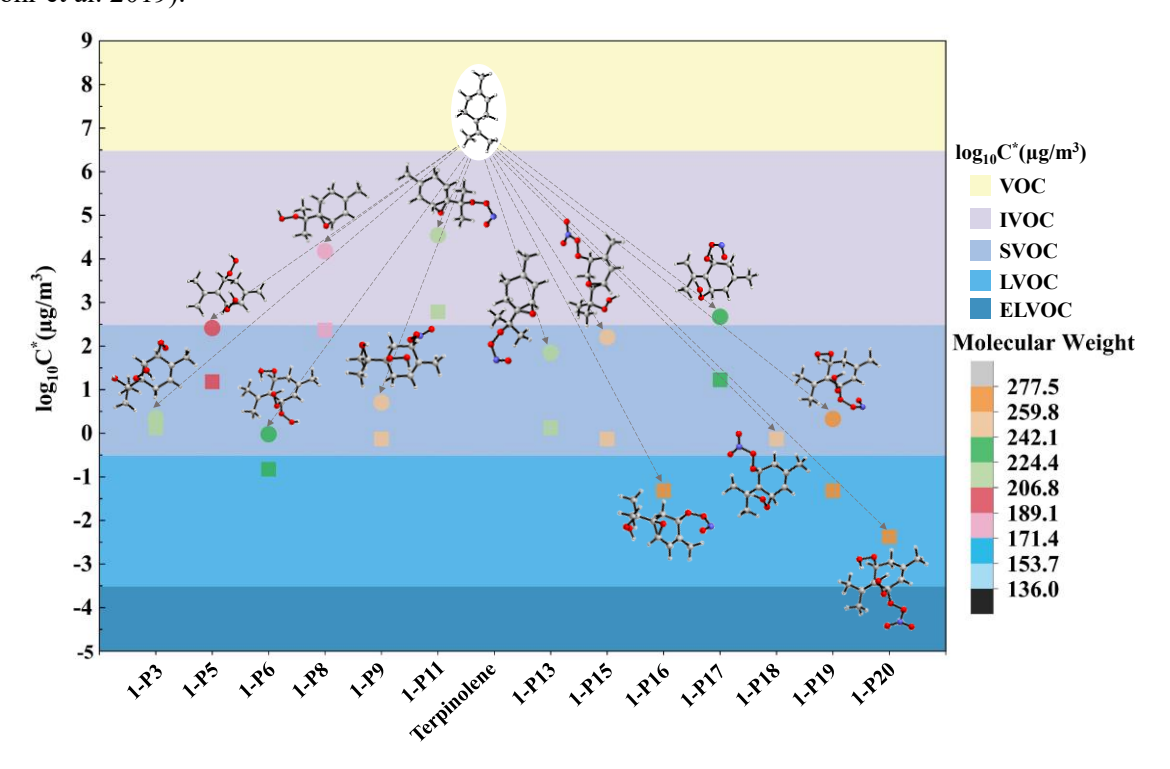


Figure 6. The molecular weight ranges and volatility classifications of C10-OOMs generated from OH-Ter-R \bullet (1-IM4 and 1-IM7) oxidation. (Volatility prediction methods: (\bigcirc) the functional group contribution method (SIMPOL.1), (\square) the molecular formula parameterization method)

As shown in Fig. 6, the OOMs generated from the oxidation of terpinolene with OH are mainly IVOC, SVOC, and LVOC. Noteworthily, the results obtained from both methods indicate that most of the OOMs belong to SVOC and LVOC, among which, 1-P6, 1-P16, 1-P19, and 1-P20 are categorized as LVOC by the molecular formula parameterization method, while 1-P6 and 1-P19 are identified as SVOC, according to the functional group contribution method. From the analysis of the atmospheric oxidation mechanism of terpinolene by OH, it can be found that these four OOMs are generated by the subsequent oxidation of the intermediate 1-IM7 produced by the H-atom abstraction reaction, and the RONO2 OOMs (1-

P16, 1-P19, and 1-P20) are produced by the reactions of peroxyl radicals with NO/NO₂. 1-P16 is generated by the reaction of NO₂ with a new peroxyl radical formed by the autoxidation of the peroxyl radical containing a C-O-C ring, which is derived from the reaction of IM7 with NO/O₂. In the previous analysis, we also emphasized the importance of this pathway for the generation of OOMs, due to the existence of C=C(CH₃)₂ double bond in the terpinolene molecule, unlike the molecular structures of the products generated from NO₂ elimination in previous studies, a C-O-C ring is formed, leading to the generation of a new alkyl radical, which is conducive to the generation of OOMs.

As revealed in Fig. 7, most of the OOMs generated from the oxidation of terpinolene by NO₃ are nitrogenous OOMs, except for 2-P12. The results obtained from the functional group contribution method indicate that the majority of the nitrogenous OOMs are within the range of SVOC, with only 2-P6, 2-P7, and 2-P19 assigned to LVOC. According to the molecular formula parameterization method, most of the RONO₂ OOMs belong to LVOC, except for 2-P19 and 2-P20 sorted as ELVOC. Concretely, 2-P6 is the oxidative product of the adduct 2-IM3 via twice H shifts (1,5- and 1,6-H shift). For the formation of 2-P7, 2-P19, and 2-P20, the alkoxyl radical 2-IM37 undergoes the cleavages of the O-N and C-C bond and the further reaction with O₂ to produce a new peroxyalkyl radical, ultimately producing 2-P7, 2-P19, and 2-P20 through 1,6-H shift, the reaction with NO and NO₂, respectively. Overall, compared to the generated OOMs induced by OH, the effective saturation concentration (C*) of OOMs derived from the oxidation by NO₃ is generally lower, being more easily distributed into the particle phase. It should be noted that there existed a significant difference in the volatile classification of 2-P14 and 2-P15 containing bicyclic structure utilizing these two methods, even crossing the SVOC range.

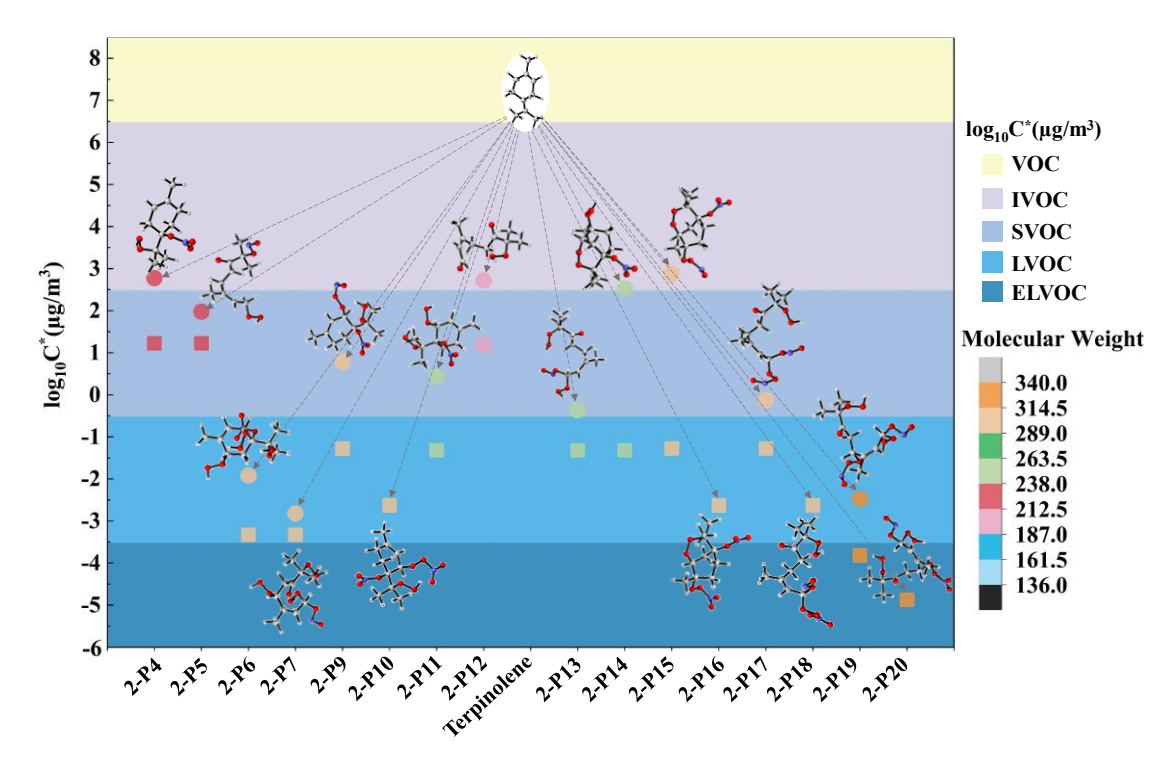


Figure 7. The molecular weight ranges and volatility classifications of C10-OOMs generated from NO₃-Ter-R• (2-IM3) oxidation. (Volatility prediction methods:(\bigcirc) the functional group contribution method(SIMPOL.1), (\square) the molecular formula parameterization method)

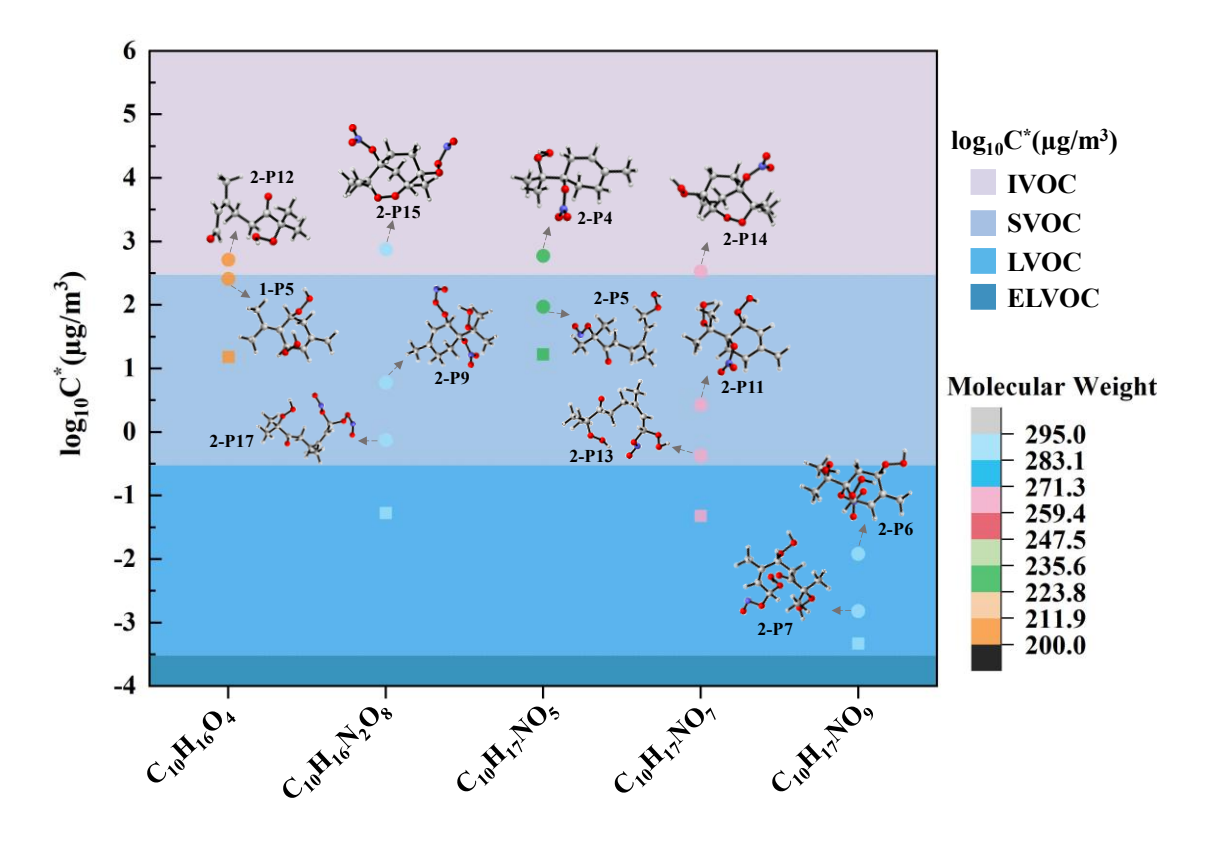


Figure 8. The molecular weight ranges and volatility classifications of C10-OOMs isomers. (Volatility prediction methods: (\bigcirc) the functional group contribution method(SIMPOL.1), (\Box) the molecular formula parameterization method)

Based on the molecular structures of each OOMs obtained from quantum chemical calculation, five groups of isomers were emphatically discussed, as shown in Fig. 8, the C* values of OOMs estimated by the molecular formula parameterization method are generally smaller compared to the results obtained from the functional group contribution method, possibly leading to a distinct underestimation of the saturated vapor pressure, which could affect the accurate assessment of the gas-particle partitioning of OOMs. By contrast, the difference in the effective saturation concentrations of the nitrogen-free OOMs (2-P12 and 1-P5) is small, while those for the other four groups of RONO2 OOMs isomers exhibit evident differences. Moreover, for the nitrogen-free OOMs (2-P12 and 1-P5), the saturated vapor pressure of 1-P5 with a cyclic structure was relatively lower. For the RONO₂ OOMs (the other four groups), the effective saturation concentrations of the isomers in each group follow the rule, i.e., the bicyclic structure > the monocyclic structure > the acyclic structure, which implies that the ring-opening reaction could have an important influence on the generation of the lowvolatile products. According to the previous findings of the vital role of isoprene nitrates in new particle formation in the upper troposphere over Amazon, the RONO₂ OOMs could contribute significantly to SOA formation (Curtius et al. 2024).

4 Conclusion and atmospheric implications

In this work, the atmospheric oxidation mechanism of terpinolene by OH and NO₃ was comprehensively investigated, expounding the formation pathways of OOMs and their molecular structures, indirectly corroborated by the available field observations and laboratory studies. Based on the reaction mechanism, the zero-dimensional chemical model was established to clarify the yield profiles of the main products including OOMs under three typical atmospheric conditions. In addition, the saturation vapor pressures of OOMs were estimated by the SIMPOL.1 method and the molecular formula parameterization method to evaluate their contributions to SOA formation.

We found that the first-generation peroxyl radical (1-IM71), resulting from the H-atom abstraction reaction pathway of terpinolene by OH, plays a pivotal role in the formation of C10OOMs. 1-IM71 can undergo twice H shift or the reaction with NO to form a cyclic peroxy radical (1-IM79), ultimately leading to the production of low volatile OOMs (such as 1-P19, 1-

P20, and 1-P16). Among the products, the yields of 1-IM76 account for the large proportions under three atmospheric conditions. Whereas, the first-generation peroxyl radical formed by the OH addition reaction of terpinolene can only proceed with one H shift continued with bond breaking, resulting in the formation of C7OOMs. According to the yield profiles, 1-P9 are the main oxidation products with yields of more than 30% in suburban and forested areas.

For the oxidation of terpinolene by NO₃, the first-generation peroxyl radical derived from NO₃ addition can also undergo H shift, followed by the cyclization, the rupture of O-N bond and C-C bond, thereby the radical center is migrated, triggering a new round of autoxidation driven by the hydrogen shift reaction to produce RONO₂ OOMs, with the total yields of 2-P18, 2-P19 and 2-P20 over 20%. Analogously, the adduct generated by NO₃ addition to terpinolene can also produce C10OOMs (2-P5) via cyclization and the cleavage of O-N and C-C bonds. Therefore, the reaction pathway of achieving the transfer of the radical center via bond breaking is a newly identified but important mechanism for the formation of OOMs except for H shift, which could be applicable to the oxidation of other terpenoids.

The generated OOMs by atmospheric oxidation of terpinolene are mainly IVOC, SVOC, LVOC, and some ELVOC, and there is a distinct difference in the effective saturation concentration of the OOM isomers. Compared with the OOMs (mostly I/SVOC) generated from the oxidation of terpinolene by OH radical, the formed RONO₂ OOMs (mainly S/LVOC) via the reaction of terpinolene with NO₃ have lower volatility with more potential to contribute to SOA formation. It could be indirectly proved by the measurements in urban atmospheres, the concentrations of organic nitrate (RONO₂) OOMs dominated the total OOMs during four seasons (Yuan et al. 2024), highlighting its significance in atmospheric chemistry.

Given the multitude of OOMs formed in the atmosphere, their molecular structures (existing numerous isomers) and formation pathways remain unclear. The findings of this work would be conducive to illuminating the formation mechanism of OOMs by terpene oxidation in the atmosphere and the measurements in the laboratory and field sites. However, it should be noted that the yields of OOMs calculated by the zero-dimensional chemical model could have some uncertainties, derived from the uneven distribution of pollutants, the neglect of advection, diffusion, and meteorological factors, incomplete chemical mechanisms, the errors of initial conditions, time step size, and numerical integration, etc. Therefore, well-integrated

- 464 models are needed to clarify the coupling of OOMs formation with multiple factors, achieving
- 465 more accurate predictions.

466 Code/Data availability

- The data and code for quantum chemical calculations and zero-dimensional chemical models
- used in this study are available upon request.

Supporting Information Available

- Detailed information on Fig. S1-S15 and Table S1-S4 is all provided in the supporting
- 471 information.

469

472 **Author contributions**

- JD and HW conceived and designed the study and wrote the original draft. HW performed the
- data analysis and created the figures; XZ, WY, ST, and SZ collected the dataset. ST and JD
- developed the model. SZ, QZ, and WW reviewed and edited the manuscript. All authors
- participated in the discussion and review of the manuscript.

477 Competing interests

The contact author has declared that none of the authors has any competing interests.

479 Acknowledgments

- 480 This work was supported by the National Natural Science Foundation of China (No. 22006095,
- 481 52106169, 22236004), the China Postdoctoral Science Foundation (No. 2021M690097), and
- 482 the Future Plan for Young Scholars of Shandong University.

483 **Reference**

- 484 Arey, J., Atkinson, R. and Aschmann, S.M. (1990) Product Study of the Gas-Phase Reactions of
- 485 Monoterpenes With the OH Radical in the Presence of NOx. Journal of Geophysical Research-
- 486 Atmospheres 95(D11), 18539-18546.
- 487 Aschmann, S.M., Arey, J. and Atkinson, R. (2002) OH radical formation from the gas-phase reactions of
- 488 O3 with a series of terpenes. Atmospheric Environment 36(27), 4347-4355.
- 489 Atkinson, R. and Arey, J. (2003) Atmospheric Degradation of Volatile Organic Compounds. Chemical
- 490 Reviews 103(12), 4605-4638.
- 491 Atkinson, R., Aschmann, S.M., Arey, J. and Shorees, B. (1992) Formation of OH Radicals in the Gas
- 492 Phase Reactions of O3 With a Series of Terpenes. Journal of Geophysical Research-Atmospheres 97(D5),

- 493 6065-6073.
- 494 Atkinson, R., Hasegawa, D. and Aschmann, S.M. (1990) Rate Constants for the Gas-Phase Reactions of
- 495 O3 with a Series of Monoterpenes and Related Compounds at 296±2 K. International Journal of
- 496 Chemical Kinetics 22(8), 871-887.
- 497 Bianchi, F., Garmash, O., He, X.C., Yan, C., Iyer, S., Rosendahl, I., Xu, Z.N., Rissanen, M.P., Riva, M.,
- Taipale, R., Sarnela, N., Petäjä, T., Worsnop, D.R., Kulmala, M., Ehn, M. and Junninen, H. (2017) The
- 499 role of highly oxygenated molecules (HOMs) in determining the composition of ambient ions in the
- boreal forest. ATMOSPHERIC CHEMISTRY AND PHYSICS 17(22), 13819-13831.
- Bianchi, F., Kurtén, T., Riva, M., Mohr, C., Rissanen, M.P., Roldin, P., Berndt, T., Crounse, J.D.,
- Wennberg, P.O., Mentel, T.F., Wildt, J., Junninen, H., Jokinen, T., Kulmala, M., Worsnop, D.R., Thornton,
- 503 J.A., Donahue, N., Kjaergaard, H.G. and Ehn, M. (2019) Highly oxygenated organic molecules (HOM)
- from gas-phase autoxidation involving peroxy radicals: A key contributor to atmospheric aerosol.
- 505 Chemical Reviews 119(6), 3472-3509.
- 506 Boyd, A.A., Flaud, P.-M., Daugey, N. and Lesclaux, R. (2003) Rate Constants for RO2 + HO2 Reactions
- Measured under a Large Excess of HO2. The Journal of Physical Chemistry A 107(6), 818-821.
- 508 Corchnoy, S.B. and Atkinson, R. (1990) Kinetics of the Gas-Phase Reactions of OH and NO3 Radicals
- with 2-Carene, 1,8-Cineole, p-Cymene, and Terpinolene. Environmental Science & Technology 24(10),
- 510 1497-1502.
- 511 Curtius, J., Heinritzi, M., Beck, L.J., Pöhlker, M.L., Tripathi, N., Krumm, B.E., Holzbeck, P.,
- Nussbaumer, C.M., Hernández Pardo, L., Klimach, T., Barmpounis, K., Andersen, S.T., Bardakov, R.,
- Bohn, B., Cecchini, M.A., Chaboureau, J.-P., Dauhut, T., Dienhart, D., Dörich, R., Edtbauer, A., Giez,
- A., Hartmann, A., Holanda, B.A., Joppe, P., Kaiser, K., Keber, T., Klebach, H., Krüger, O.O., Kürten, A.,
- Mallaun, C., Marno, D., Martinez, M., Monteiro, C., Nelson, C., Ort, L., Raj, S.S., Richter, S., Ringsdorf,
- A., Rocha, F., Simon, M., Sreekumar, S., Tsokankunku, A., Unfer, G.R., Valenti, I.D., Wang, N., Zahn,
- 517 A., Zauner-Wieczorek, M., Albrecht, R.I., Andreae, M.O., Artaxo, P., Crowley, J.N., Fischer, H., Harder,
- 518 H., Herdies, D.L., Machado, L.A.T., Pöhlker, C., Pöschl, U., Possner, A., Pozzer, A., Schneider, J.,
- Williams, J. and Lelieveld, J. (2024) Isoprene nitrates drive new particle formation in Amazon's upper
- 520 troposphere. Nature 636(8041), 124-130.
- 521 Draper, D.C., Farmer, D.K., Desyaterik, Y. and Fry, J.L. (2015) A qualitative comparison of secondary
- organic aerosol yields and composition from ozonolysis of monoterpenes at varying concentrations of
- 523 NO2. ATMOSPHERIC CHEMISTRY AND PHYSICS 15(21), 12267-12281.
- 524 Fouqueau, A., Cirtog, M., Cazaunau, M., Pangui, E., Doussin, J.F. and Picquet-Varrault, B. (2022) An
- 525 experimental study of the reactivity of terpinolene and β-caryophyllene with the nitrate radical.
- 526 ATMOSPHERIC CHEMISTRY AND PHYSICS 22(10), 6411-6434.
- 527 Friedman, B. and Farmer, D.K. (2018) SOA and gas phase organic acid yields from the sequential
- 528 photooxidation of seven monoterpenes. Atmospheric Environment 187, 335-345.
- 529 Fry, J.L., Draper, D.C., Barsanti, K.C., Smith, J.N., Ortega, J., Winkler, P.M., Lawler, M.J., Brown, S.S.,
- 530 Edwards, P.M., Cohen, R.C. and Lee, L. (2014) Secondary Organic Aerosol Formation and Organic
- Nitrate Yield from NO3 Oxidation of Biogenic Hydrocarbons. Environmental Science & Technology
- 532 48(20), 11944-11953.
- 533 Garmash, O., Rissanen, M.P., Pullinen, I., Schmitt, S., Kausiala, O., Tillmann, R., Zhao, D., Percival, C.,
- Bannan, T.J., Priestley, M., Hallquist, Å.M., Kleist, E., Kiendler-Scharr, A., Hallquist, M., Berndt, T.,
- McFiggans, G., Wildt, J., Mentel, T.F. and Ehn, M. (2020) Multi-generation OH oxidation as a source
- 536 for highly oxygenated organic molecules from aromatics. ATMOSPHERIC CHEMISTRY AND

- 537 PHYSICS 20(1), 515-537.
- 538 Griffin, R.J., Cocker, D.R., III, Flagan, R.C. and Seinfeld, J.H. (1999) Organic aerosol formation from
- the oxidation of biogenic hydrocarbons. Journal of Geophysical Research 104(D3), 3555-3567.
- 540 Guenther, A.B., Jiang, X., Heald, C.L., Sakulyanontvittaya, T., Duhl, T., Emmons, L.K. and Wang, X.
- 541 (2012) The Model of Emissions of Gases and Aerosols from Nature version 2.1 (MEGAN2.1): an
- extended and updated framework for modeling biogenic emissions. Geosci. Model Dev. 5(6), 1471-1492.
- 543 Guo, Y., Yan, C., Liu, Y., Qiao, X., Zheng, F., Zhang, Y., Zhou, Y., Li, C., Fan, X., Lin, Z., Feng, Z.,
- Zhang, Y., Zheng, P., Tian, L., Nie, W., Wang, Z., Huang, D., Daellenbach, K.R., Yao, L., Dada, L.,
- 545 Bianchi, F., Jiang, J., Liu, Y., Kerminen, V.M. and Kulmala, M. (2022) Seasonal variation in oxygenated
- organic molecules in urban Beijing and their contribution to secondary organic aerosol. ATMOSPHERIC
- 547 CHEMISTRY AND PHYSICS 22(15), 10077-10097.
- 548 Hakola, H., Arey, J., Aschmann, S.M. and Atkinson, R. (1994) Product formation from the gas-phase
- reactions of OH radicals and O3 with a series of monoterpenes. Journal of Atmospheric Chemistry 18(1),
- 550 75-102.
- Herrmann, F., Winterhalter, R., Moortgat, G.K. and Williams, J. (2010) Hydroxyl radical (OH) yields
- from the ozonolysis of both double bonds for five monoterpenes. Atmospheric Environment 44(28),
- 553 3458-3464.
- Hofzumahaus, A., Rohrer, F., Lu, K., Bohn, B., Brauers, T., Chang, C.-C., Fuchs, H., Holland, F., Kita,
- K., Kondo, Y., Li, X., Lou, S., Shao, M., Zeng, L., Wahner, A. and Zhang, Y. (2009) Amplified Trace Gas
- 556 Removal in the Troposphere. SCience 324(5935), 1702-1704.
- Huang, X., Zhou, L., Ding, A., Qi, X., Nie, W., Wang, M., Chi, X., Petäjä, T., Kerminen, V.M., Roldin,
- P., Rusanen, A., Kulmala, M. and Boy, M. (2016) Comprehensive modelling study on observed new
- particle formation at the SORPES station in Nanjing, China. ATMOSPHERIC CHEMISTRY AND
- 560 PHYSICS 16(4), 2477-2492.
- 561 Humphrey, W., Dalke, A. and Schulten, K. (1996) VMD: Visual molecular dynamics. Journal of
- 562 Molecular Graphics 14(1), 33-38.
- Isaacman-VanWertz, G. and Aumont, B. (2021) Impact of organic molecular structure on the estimation
- of atmospherically relevant physicochemical parameters. Atmos. Chem. Phys. 21(8), 6541-6563.
- Kim, H. (2016) A Density Functional Theory Study on the Reaction Mechanism of Terpinolene with O3.
- Bulletin of the Korean Chemical Society 37(2), 121-122.
- Kurtén, T., Møller, K.H., Nguyen, T.B., Schwantes, R.H., Misztal, P.K., Su, L., Wennberg, P.O., Fry, J.L.
- and Kjaergaard, H.G. (2017) Alkoxy Radical Bond Scissions Explain the Anomalously Low Secondary
- 569 Organic Aerosol and Organonitrate Yields From α-Pinene + NO3. The Journal of Physical Chemistry
- 570 Letters 8(13), 2826-2834.
- Lee, A., Goldstein, A.H., Keywood, M.D., Gao, S., Varutbangkul, V., Bahreini, R., Ng, N.L., Flagan, R.C.
- and Seinfeld, J.H. (2006) Gas-phase products and secondary aerosol yields from the ozonolysis of ten
- different terpenes. Journal of Geophysical Research-Atmospheres 111(D7).
- 574 Lindwall, F., Faubert, P. and Rinnan, R. (2015) Diel Variation of Biogenic Volatile Organic Compound
- 575 Emissions- A field Study in the Sub, Low and High Arctic on the Effect of Temperature and Light. PLOS
- 576 ONE 10(4), e0123610.
- 577 Liu, Y., Liu, C., Nie, W., Li, Y., Ge, D., Chen, L., Zhu, C., Wang, L., Zhang, Y., Liu, T., Qi, X., Wang, J.,
- Huang, D., Wang, Z., Yan, C., Chi, X. and Ding, A. (2023) Exploring condensable organic vapors and
- their co-occurrence with PM2.5 and O3 in winter in Eastern China. Environmental Science: Atmospheres
- 580 3(2), 282-297.

- 581 Liu, Y., Nie, W., Li, Y., Ge, D., Liu, C., Xu, Z., Chen, L., Wang, T., Wang, L., Sun, P., Qi, X., Wang, J.,
- Xu, Z., Yuan, J., Yan, C., Zhang, Y., Huang, D., Wang, Z., Donahue, N.M., Worsnop, D., Chi, X., Ehn,
- 583 M. and Ding, A. (2021) Formation of condensable organic vapors from anthropogenic and biogenic
- volatile organic compounds (VOCs) is strongly perturbed by NOx in eastern China. ATMOSPHERIC
- 585 CHEMISTRY AND PHYSICS 21(19), 14789-14814.
- Lu, T. and Chen, F. (2012) Multiwfn: A multifunctional wavefunction analyzer. 33(5), 580-592.
- Luo, D.M., Pierce, J.A., Malkina, I.L. and Carter, W.P.L. (1996) Rate constants for the reactions of O(3P)
- with selected monoterpenes. International Journal of Chemical Kinetics 28(1), 1-8.
- Luo, H., Vereecken, L., Shen, H., Kang, S., Pullinen, I., Hallquist, M., Fuchs, H., Wahner, A., Kiendler-
- 590 Scharr, A., Mentel, T.F. and Zhao, D. (2023) Formation of highly oxygenated organic molecules from
- 591 the oxidation of limonene by OH radical: significant contribution of H-abstraction pathway.
- 592 ATMOSPHERIC CHEMISTRY AND PHYSICS 23(13), 7297-7319.
- Ma, F., Guo, X., Xia, D., Xie, H.-B., Wang, Y., Elm, J., Chen, J. and Niu, J. (2021) Atmospheric
- 594 Chemistry of Allylic Radicals from Isoprene: A Successive Cyclization-Driven Autoxidation Mechanism.
- 595 Environmental Science & Technology 55(8), 4399-4409.
- Martínez, E., Cabañas, B., Aranda, A., Martín, P. and Salgado, S. (1999) Absolute rate coefficients for
- 597 the gas-phase reactions of NO3 radical with a series of monoterpenes at T=298 to 433 K. Journal of
- 598 Atmospheric Chemistry 33(3), 265-282.
- Mohr, C., Lopez-Hilfiker, F.D., Yli-Juuti, T., Heitto, A., Lutz, A., Hallquist, M., D'Ambro, E.L., Rissanen,
- M.P., Hao, L., Schobesberger, S., Kulmala, M., Mauldin III, R.L., Makkonen, U., Sipilä, M., Petäjä, T.
- and Thornton, J.A. (2017) Ambient observations of dimers from terpene oxidation in the gas phase:
- 602 Implications for new particle formation and growth. Geophysical Research Letters 44(6), 2958-2966.
- Mohr, C., Thornton, J.A., Heitto, A., Lopez-Hilfiker, F.D., Lutz, A., Riipinen, I., Hong, J., Donahue,
- N.M., Hallquist, M., Petäjä, T., Kulmala, M. and Yli-Juuti, T. (2019) Molecular identification of organic
- vapors driving atmospheric nanoparticle growth. Nature Communications 10(1), 4442.
- 606 Nie, W., Yan, C., Huang, D.D., Wang, Z., Liu, Y., Qiao, X., Guo, Y., Tian, L., Zheng, P., Xu, Z., Li, Y.,
- Xu, Z., Qi, X., Sun, P., Wang, J., Zheng, F., Li, X., Yin, R., Dallenbach, K.R., Bianchi, F., Petäjä, T.,
- Zhang, Y., Wang, M., Schervish, M., Wang, S., Qiao, L., Wang, Q., Zhou, M., Wang, H., Yu, C., Yao, D.,
- 609 Guo, H., Ye, P., Lee, S., Li, Y.J., Liu, Y., Chi, X., Kerminen, V.-M., Ehn, M., Donahue, N.M., Wang, T.,
- 610 Huang, C., Kulmala, M., Worsnop, D., Jiang, J. and Ding, A. (2022) Secondary organic aerosol formed
- by condensing anthropogenic vapours over China's megacities. Nature Geoscience 15(4), 255-261.
- 612 Nie, W., Yan, C., Yang, L., Roldin, P., Liu, Y., Vogel, A.L., Molteni, U., Stolzenburg, D., Finkenzeller,
- 613 H., Amorim, A., Bianchi, F., Curtius, J., Dada, L., Draper, D.C., Duplissy, J., Hansel, A., He, X.-C.,
- 614 Hofbauer, V., Jokinen, T., Kim, C., Lehtipalo, K., Nichman, L., Mauldin, R.L., Makhmutov, V., Mentler,
- B., Mizelli-Ojdanic, A., Petäjä, T., Quéléver, L.L.J., Schallhart, S., Simon, M., Tauber, C., Tomé, A.,
- Volkamer, R., Wagner, A.C., Wagner, R., Wang, M., Ye, P., Li, H., Huang, W., Qi, X., Lou, S., Liu, T.,
- 617 Chi, X., Dommen, J., Baltensperger, U., El Haddad, I., Kirkby, J., Worsnop, D., Kulmala, M., Donahue,
- 618 N.M., Ehn, M. and Ding, A. (2023) NO at low concentration can enhance the formation of highly
- oxygenated biogenic molecules in the atmosphere. Nature Communications 14(1), 3347.
- 620 Orlando, J.J., Nozière, B., Tyndall, G.S., Orzechowska, G.E., Paulson, S.E. and Rudich, Y. (2000)
- Product studies of the OH- and ozone-initiated oxidation of some monoterpenes. Journal of Geophysical
- 622 Research-Atmospheres 105(D9), 11561-11572.
- Orzechowska, G.E. (2003) Atmospheric chemistry of ozone reactions with alkenes.
- 624 Pankow, J.F. and Asher, W.E. (2008) SIMPOL.1: a simple group contribution method for predicting

- vapor pressures and enthalpies of vaporization of multifunctional organic compounds. ATMOSPHERIC
- 626 CHEMISTRY AND PHYSICS 8(10), 2773-2796.
- Peeters, J., Müller, J.-F., Stavrakou, T. and Nguyen, V.S. (2014) Hydroxyl Radical Recycling in Isoprene
- Oxidation Driven by Hydrogen Bonding and Hydrogen Tunneling: The Upgraded LIM1 Mechanism.
- The Journal of Physical Chemistry A 118(38), 8625-8643.
- 630 Qiao, X.H., Li, X.X., Yan, C., Sarnela, N., Yin, R.J., Guo, Y.S., Yao, L., Nie, W., Huang, D.D., Wang, Z.,
- Bianchi, F., Liu, Y.C., Donahue, N.M., Kulmala, M. and Jiang, J.K. (2023) Precursor apportionment of
- 632 atmospheric oxygenated organic molecules using a machine learning method. ENVIRONMENTAL
- 633 SCIENCE-ATMOSPHERES 3(1), 230-237.
- 634 Reissell, A., Harry, C., Aschmann, S.M., Atkinson, R. and Arey, J. (1999) Formation of acetone from the
- OH radical- and O3-initiated reactions of a series of monoterpenes. Journal of Geophysical Research-
- 636 Atmospheres 104(D11), 13869-13879.
- Rollins, A.W., Pusede, S., Wooldridge, P., Min, K.E., Gentner, D.R., Goldstein, A.H., Liu, S., Day, D.A.,
- Russell, L.M., Rubitschun, C.L., Surratt, J.D. and Cohen, R.C. (2013) Gas/particle partitioning of total
- 639 alkyl nitrates observed with TD-LIF in Bakersfield. Journal of Geophysical Research: Atmospheres
- 640 118(12), 6651-6662.
- 641 Saunders, S.M., Jenkin, M.E., Derwent, R.G. and Pilling, M.J. (2003) Protocol for the development of
- the Master Chemical Mechanism, MCM v3 (Part A): tropospheric degradation of non-aromatic volatile
- organic compounds. ATMOSPHERIC CHEMISTRY AND PHYSICS 3(1), 161-180.
- Shen, H., Vereecken, L., Kang, S., Pullinen, I., Fuchs, H., Zhao, D. and Mentel, T.F. (2022) Unexpected
- significance of a minor reaction pathway in daytime formation of biogenic highly oxygenated organic
- 646 compounds. Science Advances 8(42), eabp8702.
- Shu, Y. and Atkinson, R. (1994) Rate constants for the gas-phase reactions of O3 with a series of Terpenes
- and OH radical formation from the O3 reactions with Sesquiterpenes at 296 ± 2 K. International Journal
- 649 of Chemical Kinetics 26(12), 1193-1205.
- 650 Stewart, D.J., Almabrok, S.H., Lockhart, J.P., Mohamed, O.M., Nutt, D.R., Pfrang, C. and Marston, G.
- 651 (2013) The kinetics of the gas-phase reactions of selected monoterpenes and cyclo-alkenes with ozone
- and the NO3 radical. Atmospheric Environment 70, 227-235.
- 653 Surratt, J.D., Gómez-González, Y., Chan, A.W.H., Vermeylen, R., Shahgholi, M., Kleindienst, T.E.,
- 654 Edney, E.O., Offenberg, J.H., Lewandowski, M., Jaoui, M., Maenhaut, W., Claeys, M., Flagan, R.C. and
- 655 Seinfeld, J.H. (2008) Organosulfate formation in biogenic secondary organic aerosol. The Journal of
- 656 Physical Chemistry A 112(36), 8345-8378.
- 657 Tröstl, J., Chuang, W.K., Gordon, H., Heinritzi, M., Yan, C., Molteni, U., Ahlm, L., Frege, C., Bianchi,
- 658 F., Wagner, R., Simon, M., Lehtipalo, K., Williamson, C., Craven, J.S., Duplissy, J., Adamov, A., Almeida,
- J., Bernhammer, A.-K., Breitenlechner, M., Brilke, S., Dias, A., Ehrhart, S., Flagan, R.C., Franchin, A.,
- Fuchs, C., Guida, R., Gysel, M., Hansel, A., Hoyle, C.R., Jokinen, T., Junninen, H., Kangasluoma, J.,
- Keskinen, H., Kim, J., Krapf, M., Kürten, A., Laaksonen, A., Lawler, M., Leiminger, M., Mathot, S.,
- Möhler, O., Nieminen, T., Onnela, A., Petäjä, T., Piel, F.M., Miettinen, P., Rissanen, M.P., Rondo, L.,
- Sarnela, N., Schobesberger, S., Sengupta, K., Sipilä, M., Smith, J.N., Steiner, G., Tomè, A., Virtanen, A.,
- Wagner, A.C., Weingartner, E., Wimmer, D., Winkler, P.M., Ye, P., Carslaw, K.S., Curtius, J., Dommen,
- 665 J., Kirkby, J., Kulmala, M., Riipinen, I., Worsnop, D.R., Donahue, N.M. and Baltensperger, U. (2016)
- The role of low-volatility organic compounds in initial particle growth in the atmosphere. Nature
- 667 533(7604), 527-531.
- Valorso, R., Aumont, B., Camredon, M., Raventos-Duran, T., Mouchel-Vallon, C., Ng, N.L., Seinfeld,

- 669 J.H., Lee-Taylor, J. and Madronich, S. (2011) Explicit modelling of SOA formation from α-pinene
- 670 photooxidation: sensitivity to vapour pressure estimation. ATMOSPHERIC CHEMISTRY AND
- 671 PHYSICS 11(14), 6895-6910.
- Vasudevan-Geetha, V., Tiszenkel, L., Wang, Z., Russo, R., Bryant, D., Lee-Taylor, J., Barsanti, K. and
- 673 Lee, S.H. (2024) Isomer Molecular Structures and Formation Pathways of Oxygenated Organic
- Molecules in Newly Formed Biogenic Particles. EGUsphere 2024, 1-20.
- Wang, J., Feng, L., Palmer, P.I., Liu, Y., Fang, S., Bösch, H., O'Dell, C.W., Tang, X., Yang, D., Liu, L.
- and Xia, C. (2020) Large Chinese land carbon sink estimated from atmospheric carbon dioxide data.
- 677 Nature 586(7831), 720-723.
- Wang, S. and Wang, L. (2016) The atmospheric oxidation of dimethyl, diethyl, and diisopropyl ethers.
- The role of the intramolecular hydrogen shift in peroxy radicals. Physical Chemistry Chemical Physics
- 680 18(11), 7707-7714.
- Wang, Y., Clusius, P., Yan, C., Dällenbach, K., Yin, R., Wang, M., He, X.-C., Chu, B., Lu, Y., Dada, L.,
- Kangasluoma, J., Rantala, P., Deng, C., Lin, Z., Wang, W., Yao, L., Fan, X., Du, W., Cai, J., Heikkinen,
- L., Tham, Y.J., Zha, Q., Ling, Z., Junninen, H., Petäjä, T., Ge, M., Wang, Y., He, H., Worsnop, D.R.,
- Kerminen, V.-M., Bianchi, F., Wang, L., Jiang, J., Liu, Y., Boy, M., Ehn, M., Donahue, N.M. and Kulmala,
- 685 M. (2022) Molecular Composition of Oxygenated Organic Molecules and Their Contributions to Organic
- Aerosol in Beijing. Environmental Science & Technology 56(2), 770-778.
- Witter, M., Berndt, T., Böge, O., Stratmann, F. and Heintzenberg, J. (2002) Gas-phase ozonolysis:: Rate
- coefficients for a series of terpenes and rate coefficients and OH yields for 2-methyl-2-butene and 2,3-
- dimethyl-2-butene. International Journal of Chemical Kinetics 34(6), 394-403.
- 690 Wu, R., Wang, S. and Wang, L. (2015) New Mechanism for the Atmospheric Oxidation of Dimethyl
- 691 Sulfide. The Importance of Intramolecular Hydrogen Shift in a CH3SCH2OO Radical. The Journal of
- 692 Physical Chemistry A 119(1), 112-117.
- 693 Zheng, P., Chen, Y., Wang, Z., Liu, Y., Pu, W., Yu, C., Xia, M., Xu, Y., Guo, J., Guo, Y., Tian, L., Qiao,
- 694 X., Huang, D.D., Yan, C., Nie, W., Worsnop, D.R., Lee, S. and Wang, T. (2023) Molecular
- 695 Characterization of Oxygenated Organic Molecules and Their Dominating Roles in Particle Growth in
- Hong Kong. Environmental Science & Technology 57(20), 7764-7776.

697 Graphical Abstract

